Electronic structure of calcium clusters

Jeffrey W. Mirick, Chang-Hong Chien, and Estela Blaisten-Barojas*

School of Computational Sciences, George Mason University, Fairfax, Virginia 22030

The electronic structure of calcium clusters containing up to 13 atoms is studied within the general gradient approximation (GGA) of the density-functional formalism. For the calcium dimer it is observed that the exchange functional in GGA overestimates the binding energy, while a hybrid approach including Hartree-Fock exchange gives a better agreement with the experimental results. Binding energies, optimized geometries, vibrational frequencies, and thermodynamic properties have been calculated for several isomers at each cluster size. Various structures corresponding to saddle points of the energy curve are reported, along with the isomerization reaction path for Ca_5, Ca_6, and Ca_7. It was found that Ca_{12} undergoes a structural transition as a function of temperature, changing structure at $T=317$ K. A comparison of the minimum energy isomer geometry and binding energy obtained for each cluster size with those obtained from the Murrell-Mottram empirical potential shows that this potential overestimates the binding energies and does not adequately predict the optimized structures for several cluster sizes.

I. INTRODUCTION

Calcium is a very abundant element that plays an important role in a variety of compounds, mechanisms, and processes. This element is of interest because of its potential use in excimer lasers, carbon-chemical engineering, and ion deposition. Despite its popular chemical usages, only a limited number of experimental observations for pure calcium clusters [1] have been reported. Calcium belongs to the group-IIA alkaline-earth metals with closed-shell electronic configuration $[Ar]4s^2$. The bonding in the bulk quasimetal is quite strong with a cohesive energy of 1.825 eV. In contrast, the Ca_2 molecule presents a weakly bound ground state with a dissociation energy of only 0.14 eV and strongly bound excited states [2,3]. The discrepancy in the bonding behavior at the two size limits (bulk and dimer) suggests that a change in the bonding must take place as a function of cluster size.

Metallic clusters have been the subject of intense interest in recent years [4,5]. One property of small metallic clusters that has received little attention is their vibrational spectra. Recently we have reported a detailed theoretical investigation of the harmonic vibrational frequencies of Rh_2 through Rh_6 using density functional and large basis sets [6]. For small calcium clusters there have been very few *ab initio* calculations that include electron correlation effects or report vibrational frequencies: Ca_2 [7–10], Ca_3 [11], Ca_4 [9–13], and Ca_5 [9]. For larger calcium clusters there are no first-principles calculations, although there have been attempts to model the cluster geometries with the empirical potential of Murrell and Mottram (MM) [14,15] that has two- and three-body interactions.

In this paper we perform an exhaustive all-electron study within the density-functional theory (DFT) framework and the generalized gradient approximation (GGA) of Ca clusters containing up to 13 atoms. Results are presented in Sec. II

for the calcium dimer including a thorough comparison between various calculation methods. The energetics and vibrational frequencies for Ca_3 through Ca_{13} are described in Secs. III and IV. These sections also discuss several isomerization reaction paths and report several cluster structures corresponding to saddles of the energy surface. Section V contains a discussion on the thermodynamic properties obtained in the harmonic approximation and their role in the relative stability of the clusters as a function of size and temperature. A thermally induced structural transition for Ca_{12} is highlighted in this section. Concluding remarks are given in the last section of this paper.

II. METHODS AS APPLIED TO THE CALCIUM DIMER

The Kohn-Sham equations [16] were solved self-consistently using the GGA representation of the correlation functional. Becke's three-parameter functional [17] is a hybrid method that includes a combination of Hartree-Fock (HF) exchange with DFT correlation energies. The hybrid Becke–Perdew-Wang 1991 (B3PW91) method used throughout this paper includes Perdew and Wang local and non local correlation functionals [18,19]. A triple valence basis set (6-311G) containing $8s,7p,1d$ Gaussians contracted as (62111111,3311111,3) and augmented with one d polarization function [20] was used in all calculations. We found this basis set to be sufficiently large to give good results at a reasonable computational effort. Adding an additional diffuse function produced insignificant changes in both the energy and bond length of Ca_2. The basis set superposition error (BSSE) [21] was negligible for both calculations with the triple valence basis set including one or two polarization functions.

Based on the dimer results, all calculations reported in this paper were performed with the triple valence basis set including one d polarization function. Results in forthcoming sections do not include the BSSE correction. However, we

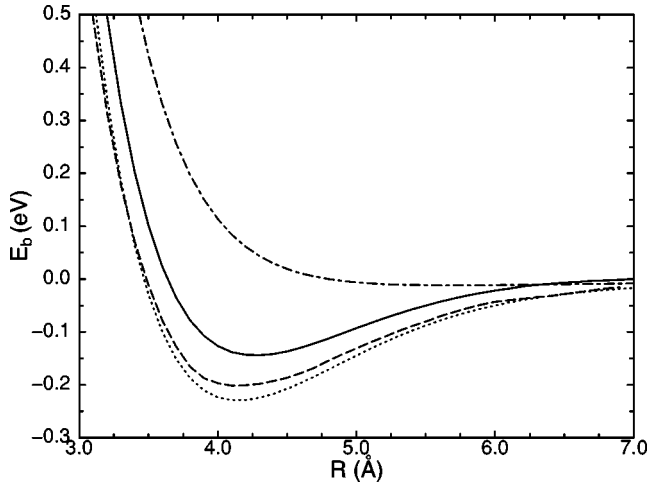---

*Email address: eblaiste@gmu.edu

FIG. 1. Binding energy of Ca_2 as a function of interatomic distance with various methods: B3PW91 (solid line), PW91PW91 (dotted), NRLMOL (dashed), and MP4 (dashed-dotted).

did test for BSSE with calculations up to Ca_4 and found an insignificant decrease in the total energy for these cluster sizes. Worth noting is that BSSE is important when the basis set is small, and our basis set is large.

Since Ca_2 is a closed-shell system, it demands a good representation of the electron correlation energy to obtain reasonable total energies. We performed an analysis of various methods on the calcium dimer, which are summarized in Fig. 1, where the binding energy (E_b) is displayed as a function of interatomic distance (R). The binding energy is computed as the value of the total energy of the dimer minus the total energy of two isolated Ca atoms (with the BSSE correction). The solid line shows results with the hybrid B3PW91 method. The dot-dashed line represents the Moller-Plesset results with up to four excitations (MP4) [22]. The dotted line illustrates results within GGA in which both exchange and correlation functionals [18,19] are provided (PW91PW91) and the same basis set as in B3PW91 was used. All calculations were done using GAUSSIAN-98 [23]. The accuracy attained in the self-consistent field (SCF) process assures eight decimal places in the energies. The dashed line pertains to the same level of approximation than PW91PW91 but results were obtained with the NRLMOL package [24]. In this case we used a basis set of 19 noncontracted Gaussians augmented by three floating Gaussians [25] to expand each of the s,p, and d orbitals that were optimized on the calcium atom. The accuracy in the SCF was the same as that obtained with the GAUSSIAN package. The small discrepancies between results obtained from using PW91PW91 (dotted line) and the NRLMOL (dashed lines) are due to the difference in the basis sets.

The MP4 calculation (dashed-dotted line) significantly underestimates the electron correlation, while GGA (both PW91PW91 and NRLMOL) overestimates the binding energy (dotted and dashed lines). The dissociation energy found with B3PW91 (solid line) is 0.147 eV, in very good agreement with the experimental result of 0.136 eV [2,3]. In addition, we found a value of 4.269 Å for the equilibrium bond

TABLE I. Comparison of different calculations of the binding energy, interatomic distance, and harmonic frequency of Ca_2.

	Method|basis set	E_b (eV)	R_e (Å)	ν (cm^{-1})
This work	B3PW91 6-311g(d)	0.144	4.27	72.3
This work	NRLMOL	0.201	4.30	76.0
Ref. [3]	Experimental	0.136	4.277	65.07
Ref. [2]	Experimental	0.133	4.28	64.93
Ref. [9]	CI [4s2p]	0.007	6.509	
Ref. [10]	CI [4s2p1d]	0.029	5.080	
Ref. [8]	LDA [4s3p]	0.012	5.503	
Ref. [7]	LDA	0.2	4.30	80

length, which compares well to the experimental value of 4.277 Å. Our predicted harmonic frequency is 72.3 cm^{-1}, also in good agreement with the experimental results. The zero-point energy correction to the binding energy is very small (0.2 kcal/mole). The first and second ionization potentials of Ca_2 calculated with B3PW91 are 4.950 and 9.118 eV, respectively.

Additionally, we performed a fit of the Morse potential parameters to the B3PW91 energy curve of Fig. 1 in the range of interatomic distances $3.3\text{Å} \leq R \leq 5.3$ Å. The values obtained are: $D_e = 0.139\,140$ eV, $\beta = 1.093$, and $r_0 = 4.261$ Å. The error of the fit was 0.01 eV (twice the standard deviation). The harmonic frequency and anharmonic constant obtained from this Morse potential are $\nu_e = 68.85$ cm^{-1} and $x_e \omega_e = 1.06$ cm^{-1}, respectively. These values are in excellent agreement with those obtained from spectroscopic measurements [2,3,26]. A fit of the long-range portion of the binding energy as a function of interatomic distance to expressions of the type R^{-6} was not successful, indicating that the dimer attractive tail carries components other than dispersive force contributions.

The PW91PW91 and the NRLMOL results are very close to the early local-density approximation (LDA) results of Jones [7]. Other calculations for the dimer have reported significantly different binding energies and interatomic distances. A summary of all results is given in Table I. We have shown that MP4 configuration interaction calculation does not include a large enough set of configurations to account for the electron correlation energy in the calcium dimer. The HF description of the electron exchange energy in Ca_2 provided by B3PW91 is superior to the functional representation of that energy in both PW91PW91 and NRLMOL. The agreement between the B3PW91 calculations and the experimental values of the binding energy, bond distance, and harmonic frequency for the calcium dimer led us to use the hybrid method B3PW91 in our investigation of larger calcium clusters.

III. ENERGETICS AND VIBRATIONAL FREQUENCIES OF CALCIUM TRIMER, TETRAMER, AND PENTAMER

Table II lists the binding energy per atom E_b, average bond length R_{ave}, energy difference between the (LUMO)

TABLE II. Binding energy per atom, HOMO-LUMO energy gap, average bond length, and harmonic frequencies of stable isomers of Ca_3, Ca_4, and Ca_5.

	Sym	E_b (eV/atom)	Δ_{HL} (eV)	R_{ave} (Å)	ν (cm^{-1})
Ca_3	D_{3h}	0.220 (B3PW91)	1.926	3.933	98.8(E'), 107.7(A_1')
		0.247 (NRLMOL)		4.171	95(E'), 109(A_1')
		0.009 Ref. [9]		6.033	
		0.162 Ref. [11]		4.172	83.0(E'), 94.0(A_1')
	$D_{\infty h}$	0.114 (B3PW91)	1.657	4.202	6.7(Π_u), 56.2 (Σ_g), 98.1(Σ_u)
		0.149 (NRLMOL)		4.200	
		0.014 Ref. [9]		6.403	
Ca_4	T_d	0.444 (B3PW91)	1.990	3.767	103.6(E), 122.7(T_2),142.0(A_1)
		0.445 (NRLMOL)		3.906	91(E), 111(T_2),130(A_1)
		0.021 Ref. [9]		5.345	
		0.151 Ref. [10]		4.286	
		0.198 Ref. [12]		4.159	
		0.199 Ref. [13]		4.138	
		0.341 Ref. [11]		4.017	86.0(E), 105.0(T_2), 127.0 (A_1)
	D_{4h}	0.075 Ref. [9]		5.874	
	$D_{\infty h}$	0.139 (B3PW91)	1.350	4.166	4.5, 4.5, 9.3, 46.1, 82.1, 114.0
		0.176 (NRLMOL)		4.452	
	D_{2h}	0.020 (B3PW91)	0.299	3.506, 3.921	
		0.046 Ref. [9]		5.980	
Ca_5	D_{3h}	0.479 (B3PW91)	1.451	3.822	69.7(E'), 87.5(E''), 91.2(A_1'), 103.4(A_2''), 132.9(E'), 157.5(A_1')
		0.483 (NRLMOL)		4.025	63(E'), 76(E''), 90(A_1'), 102(A_2''), 117(E'), 145(A_1')
		0.142 Ref. [9]		5.398	
	C_{4v}	0.087 Ref. [9]		5.715	
	C_{2v}	0.065 Ref. [9]		5.926	
	D_{5h}	0.033 Ref. [9]		6.191	

and (HOMO) one-electron levels Δ_{HL}, and normal mode frequencies. In this table, as well as in the rest of this paper, binding energies at the minima are reported as positive values. In all calculations, the self-consistent-field results (SCF) convergence was attained up to eight decimals. The optimization of the bond lengths is accurate up to four decimals. The ground-state configurations are the equilateral triangle (D_{3h}) for Ca_3, the tetrahedron (T_d) for Ca_4, and the trigonal bipyramid (D_{3h}) for Ca_5. Other geometries of the trimer and tetramer were also studied, as listed in Table II. For comparison this table contains all other published results for these cluster sizes. Previous calculations performed on Ca_3 (equilateral triangle) and Ca_4 (tetrahedron) [11] revealed a binding energy of 0.162 eV/atom and 0.341 eV/atom, respectively. Both values underestimate the binding energy as compared to our results by 30% and 26%, respectively. Reported bond lengths for the trimer and tetramer from Ref. [11] are 4.172 and 4.016 Å, respectively. These bond lengths are higher than our values of 3.933 and 3.767 Å. The pentamer is the characteristic trigonal bipyramid of close-packed structures. Reported binding energies in Ref. [9] are much lower than our results, and the corresponding bond lengths longer than our values (see Table II). Even though there are reported calculations for other geometries of Ca_4 and Ca_5 [9] as listed in Table II, none of those structures was found to be

a minimum of the energy surface. In fact, we found that most of these structures are associated with saddle points of the energy surface.

In summary, it is apparent that for the trimer and tetramer, a good treatment of both correlation and exchange energies is crucial. Not only binding energies are higher in our paper than previously reported in the literature, but also the bond lengths are significantly smaller. The HOMO-LUMO gap in the most stable isomers of Ca_3 through Ca_5 is high (1.9 to 1.4 eV), indicating that these clusters are far from presenting a metallic character. However, the gap decreases in the higher-energy isomers of these cluster sizes, as can be seen from data in Table II. When we compare our results between B3PW91 and NRLMOL (Table II), we see that the binding energies tend to have the same value, although the interatomic distances are slightly longer in NRLMOL than in B3PW91. We attribute this effect to the differences in the exchange energy between the two methods.

IV. ENERGETICS AND VIBRATIONAL FREQUENCIES OF LARGER CALCIUM CLUSTERS

The search of stable structures of Ca_6 through Ca_{13} was initialized from numerous geometries in our database. Optimization of all cluster structures was performed without

TABLE III. Binding energy per atom, HOMO-LUMO energy gap, average bond length of stable isomers of Ca_6 through Ca_{13} using B3PW91 and NRLMOL (when explicitly mentioned).

	Sym	E_b (eV/atom)	Δ_{HL} (eV)	R_{ave} (Å)
Ca_6	C_{2v}	0.514	1.217	3.852
	C_{2v}	0.520 (NRLMOL)		3.986
Ca_7	D_{5h}	0.623	1.416	3.805
	D_{5h}	0.604 (NRLMOL)		3.954
	C_2	0.563	1.283	3.851
	C_s	0.547	1.336	3.864
	C_{3v}	0.515	1.139	3.923
Ca_8	C_s	0.638	1.192	3.828
	C_s	0.629 (NRLMOL)		3.921
Ca_9	C_{2v}	0.687	1.048	3.830
	C_s	0.658	1.053	3.829
Ca_{10}	C_{4v}	0.752	1.636	3.868
	C_s	0.693	1.019	3.841
	C_s	0.659	0.835	3.865
Ca_{11}	D_{4d}	0.751	0.846	3.789
	C_1	0.733	1.026	3.842
Ca_{12}	C_1	0.756	0.900	3.848
	C_1	0.748	0.766	3.884
	C_1	0.742	0.714	3.867
Ca_{13}	C_1	0.781	0.772	3.848
	C_i	0.755	0.723	3.934

symmetry constraints. The ground state of all clusters were singlets. Accuracy in the SCF ensures eight decimal places in the energies, whereas optimization of geometries are accurate up to the fourth decimal. In Table III we report the geometry, point group, binding energy, energy gap between the LUMO and HOMO (Δ_{HL}), and average bond length for
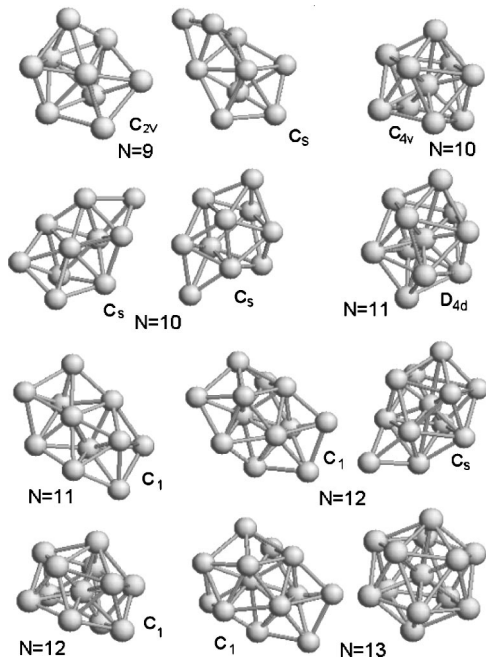

FIG. 2. Low-energy stable isomers of Ca_9 through Ca_{13}.
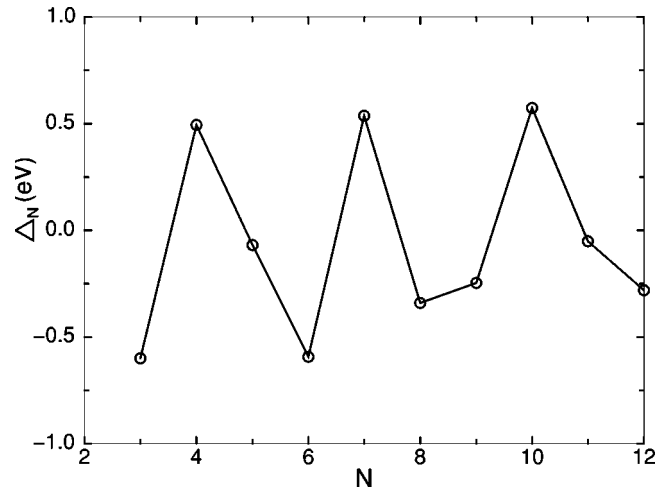

FIG. 3. Energy stability pattern of calcium clusters at zero temperature.

the investigated cluster structures of Ca_6 through Ca_{13}. The geometry of these clusters is visualized in Fig. 2. The close-packed growth sequence leading to fivefold symmetry clusters is obtained from Ca_4 through Ca_9, namely, decorating a face of the tetrahedron (Ca_4) with one atom leads to Ca_5 (trigonal bipyramid), Ca_6 is the pentamer with one decorated face, the pentagonal bipyramid is the geometry for Ca_7, the heptamer with one decorated face becomes Ca_8, and Ca_9 is the heptamer with two decorated faces. However, this sequence changes at Ca_{10}, which is the anticube with one central atom and one extra atom decorating a square face. A fourfold axis of rotation is preserved at Ca_{11} as can be seen in Fig. 2. It is also apparent from this figure that from Ca_{11} and up, a secondary structure with twinned pentagonal bipyramids is close in energy to the global minimum structure. The pentagonal bipyramid is a possible building block for larger cluster sizes. In fact the lowest-energy structure of Ca_{12} is composed of two of these building blocks with one decorated face, and the lowest structure we found for Ca_{13} is that of two twinned pentagonal bipyramids with two deco-
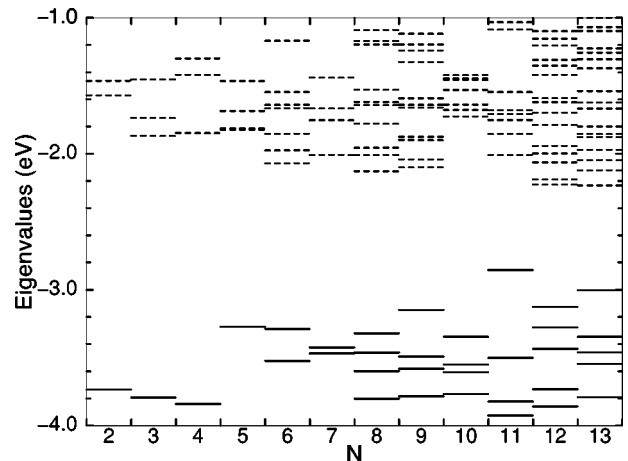

FIG. 4. One electron eigenvalues versus cluster size. Solid lines are the occupied states and dashed lines represent the virtual states.

TABLE IV. Binding energy per atom, order of saddle point, and average bond length of structures at saddle points found for Ca_4 through Ca_{10} using B3PW91.

	Sym	Order	E_b (eV/atom)	R_{ave} (Å)
Ca_4	D_{2h}	1	0.257	3.988
	D_{4h}	2	0.152	4.234
Ca_5	C_{4v}	1	0.339	3.965
Ca_6	D_{2h}	1	0.495	3.823
	D_{4h}	3	0.458	3.762
	O_h	5	0.354	4.071
	D_{6h}	6	0.178	4.182
Ca_7	C_s	1	0.549	3.824
	O_h	9	0.293	3.7
Ca_8	C_{2v}	1	0.607	3.862
	C_s	1	0.601	3.818
	D_{6h}	1	0.541	3.856
	D_{4d}	2	0.533	3.900
	D_{4h}	6	0.390	3.826
Ca_9	C_s	1	0.641	3.715
	C_{4v}	1	0.630	3.873
Ca_{10}	D_{3h}	2	0.751	3.809
	D_{4d}	2	0.640	3.899
Ca_{13}	C_1	1	0.774	3.872

rated faces. An icosahedrallike Ca_{13} (C_1 structure, not perfect icosahedron) is 0.336 eV above this twinned structure. Calculations with the NRLMOL package were also carried out for sizes up to $N=8$. The results are given in Table III. It is seen that the binding energies tend to coincide between the two calculations as the size of the cluster increases, although structures calculated with NRLMOL are systematically more expanded.

Figure 3 illustrates the second differences of the cluster binding energy, $\Delta_N = 2E_b(N) - E_b(N-1) - E_b(N+1)$, for the lowest-energy structures reported in Tables II and III. This function is a measure of the relative stability of clusters
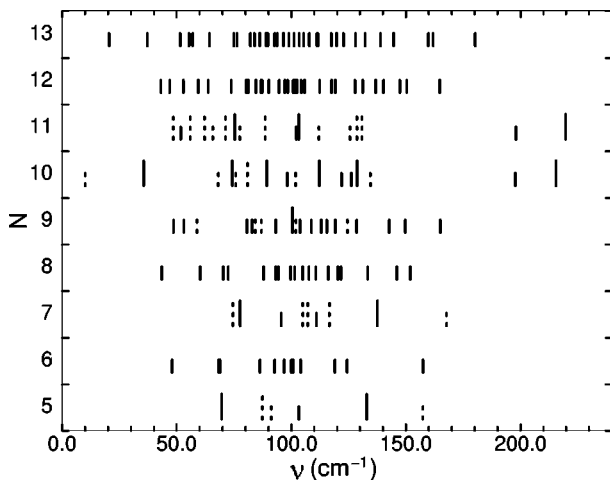

FIG. 5. Normal-mode frequencies of vibration for Ca_5 through Ca_{13}. The height of the spikes indicate the degeneracy of the mode. Solid lines are infrared active modes and dashed lines are inactive.
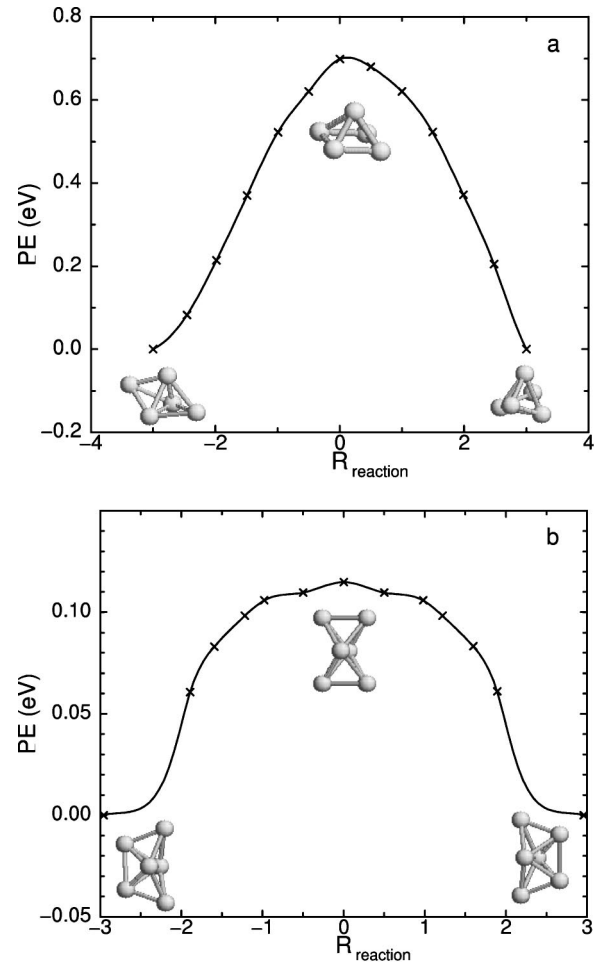

FIG. 6. Isomerization reaction paths for (a) Ca_5 and (b) Ca_6. The intermediate structure is depicted at the barrier point. Energies are relative to the energy of the corresponding reactant. The reaction coordinate is dimensionless.

at zero temperature with respect to their neighboring sizes. Peaks of this function indicate when a cluster with N atoms is relatively more stable than clusters with either $N+1$ or $N-1$ atoms. In this size range 4, 7, and 10 display an enhanced energy stability at zero temperature.

As is seen in Tables II and III, the HOMO-LUMO energy gap decreases with increasing cluster size from 1.9 for the trimer to 0.8 eV for Ca_{13}. This energy gap gives an indication of how metallic the system is, since the Fermi energy lays in it. We conclude that small clusters up to Ca_{13} are not metallic because the energy gap is an order of magnitude larger than thermal energies attainable in experiments. Figure 4 is a representation of the one-electron energies around this gap. The plot gives a visual description of how the conduction band builds up as a function of size. It is to be noted that the density-of-states of bulk fcc calcium, calculated with equivalent methods [27], indicates that the Fermi level is located in a region of low density almost edging a small gap of 0.029 eV. Tables II and III report also the average bond distance in each cluster. With the exception of Ca_4, which is more tightly bound, these averaged bond distances are slowly increasing and will eventually reach the nearest-
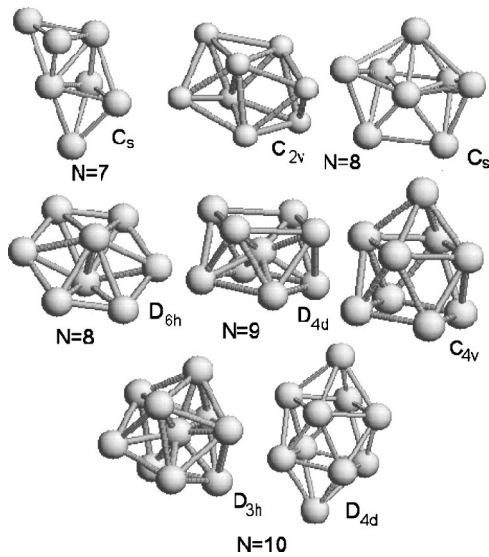
FIG. 7. Several structures of Ca_7 through Ca_{10} corresponding to saddle points of the energy surfaces.
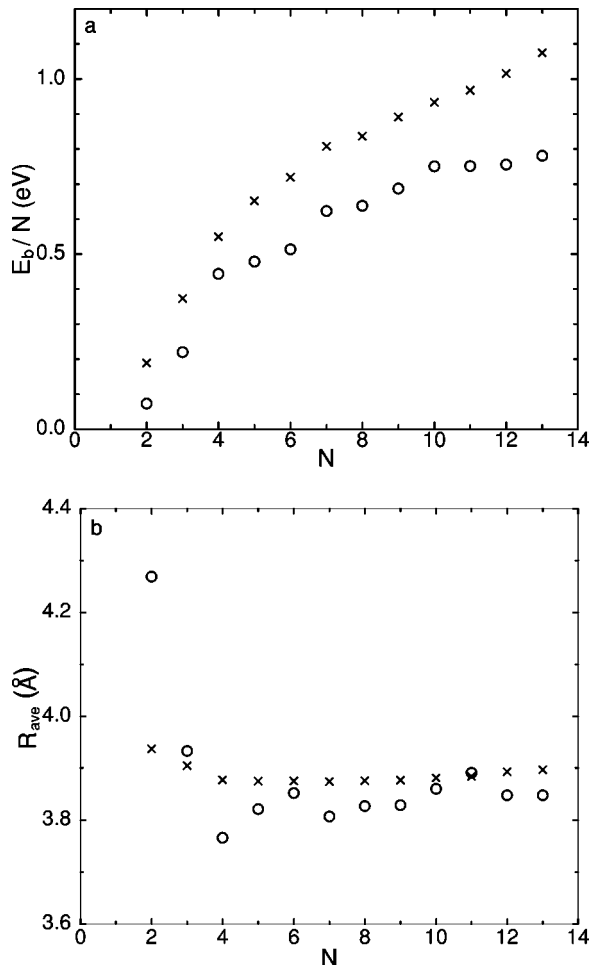

FIG. 8. Comparison of B3PW91 (circles) and Murrell-Mottram potential (crosses) of (a) binding energy per atom versus cluster size and (b) average bond length versus cluster size.
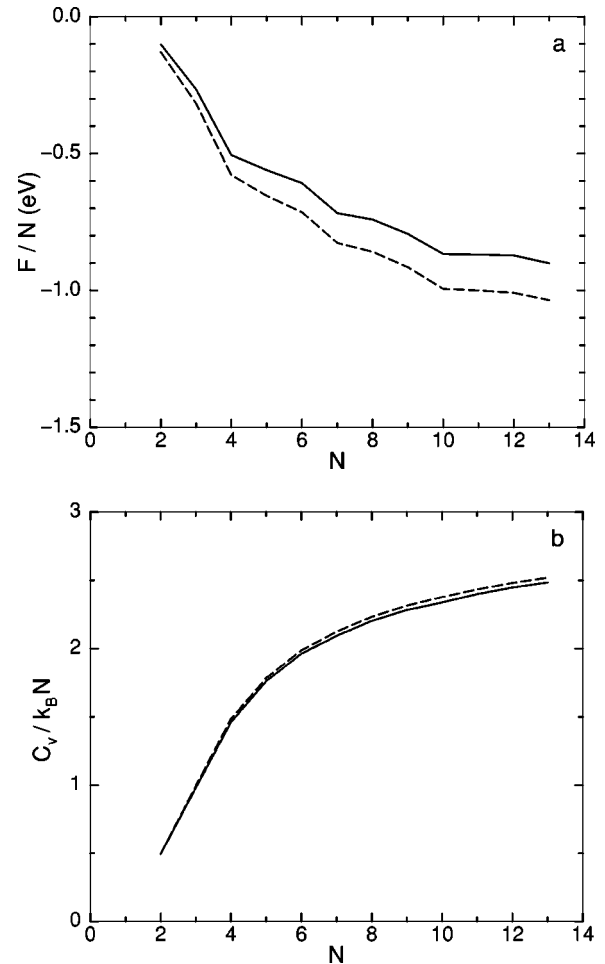

FIG. 9. (a) Free energy per atom versus cluster size; (b) specific heat versus cluster size. $T = 300$ K (full line) and $T = 500$ K (dashed line). k_B is Boltzmann's constant.

neighbor distance of 3.94 Å of bulk fcc calcium. For a given cluster size this average bond length changes with the symmetry of the isomer, as indicated in Table III.

Tables V and VI of the Appendix contain the harmonic frequencies for all the structures listed in Tables II and III. A pictorical representation of the vibrational spectrum as a function of cluster size is provided in Fig. 5. In this figure the height indicates the degeneracy of each frequency and the dashed spikes denote vibrational modes that are infrared inactive. The spectrum becomes more dense in the center of the band as the size of the cluster is increased. There is also an increase in the width of the band with cluster size. In this size range only Ca_{10} presents a very low-frequency mode.

In the search of the structures with lowest total energy we found several structures associated with saddles of the energy surface (one or multiple imaginary frequencies). Relevant data for these structures is provided in Table IV including the order of the saddle point. These structures are interesting because they might be good candidates for intermediate structures in isomerization reactions. For example, we have determined the reaction path that connects the energy surfaces of two degenerate Ca_5 (D_{3h}) isomers. We also
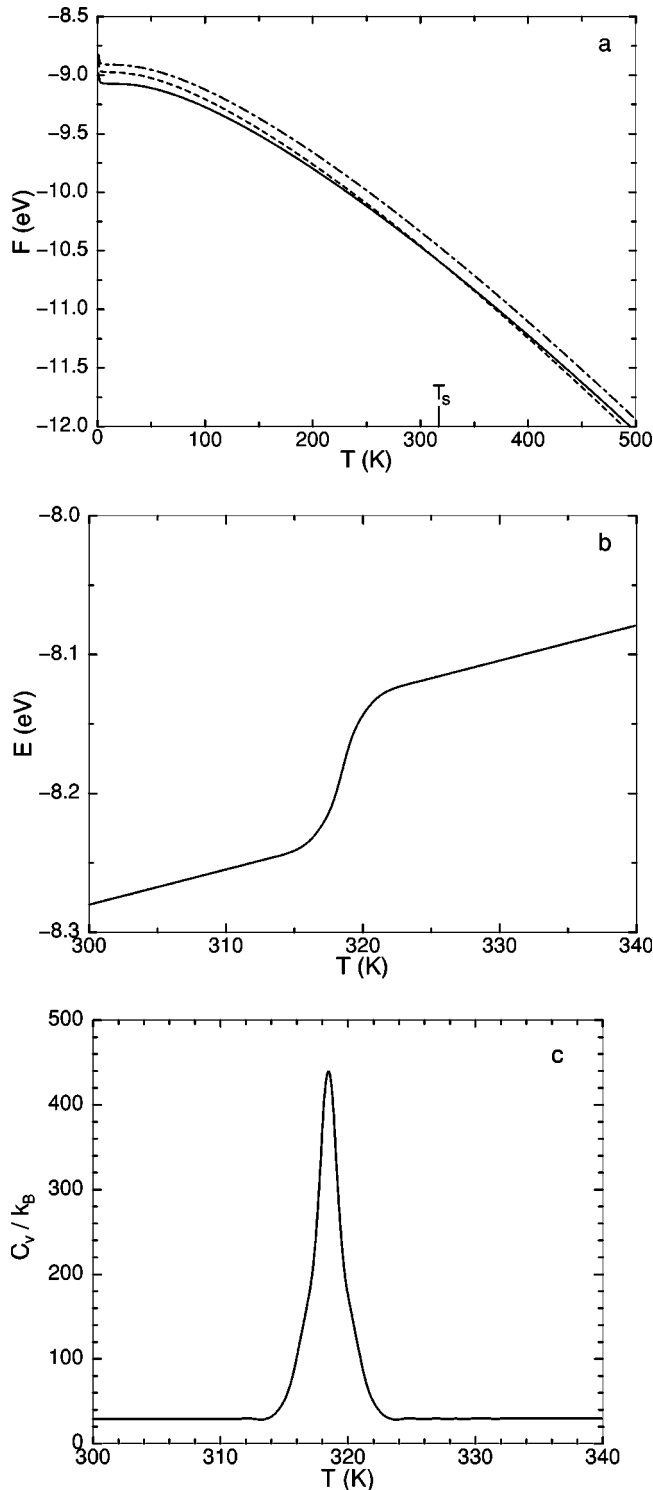
FIG. 10. Ca_{12}: (a) free energy as a function of temperature; (b) internal energy near the structural transition temperature; and (c) specific heat near the structural transition temperature. k_B is Boltzmann's constant.

found the reaction path in the isomerization of Ca_6 (C_{2v}). These reaction paths are depicted in Figs. 6(a) and 6(b) where the reported energy is relative to the binding energy of the degenerate minima. The Arrhenius-type energy barriers in the two isomerization reactions are the difference between

the binding energies of the transition structures (C_{4v} for the pentamer and D_{2h} for the hexamer reported in Table IV) minus the binding energy of the minimum structures from Tables II and III. In the case of the hexamer, the octahedron (O_h) is the stable geometry obtained under several empirical potentials including the MM potential. We have found that this geometry corresponds to a saddle point of order 5. For larger isomers, various other geometries corresponding to saddles of different orders were detected. These are illustrated in Fig. 7. The binding energies of these saddle structures (see Table IV) allow for determination of the barriers in isomerization reactions. However, these saddles do not necessarily connect the lowest-energy isomer of a given size with another isomer of higher energy. For example, one of the low-energy isomers of Ca_7 is Ca_6 with one decorated face (C_2, two intertwined trigonal bipyramids with one decorated face). There are three equivalent ways to decorate Ca_6 and therefore three equivalent isomers. In order to go from one of these isomers to the other, the reaction path needs to overcome a barrier of about 0.1 eV and the intermediate structure corresponding to the saddle point is given in Fig. 7.

For comparison purposes we reproduced the lowest-energy geometries of isomers obtained from the MM potential parametrized for calcium [15]. It was found that this potential gives the right geometry of the global minimum structure (but not the bond lengths) of Ca_3 through Ca_5 and Ca_7 through Ca_9. However, the lowest-energy isomers obtained with the MM potential for Ca_6 and Ca_{10} through Ca_{13} were different than those obtained in our work. Additionally, we found that some of the MM lowest-energy geometries are associated to saddle points. Such is the case of Ca_6 (O_h). The MM Ca_{10} structure was not stable and relaxed into the D_{3d} saddle geometry. The MM binding energies for all sizes are systematically higher than our results as is illustrated in Fig. 8(a), where the binding energy from MM structures (crosses) are compared to our calculation (circles). Figure 8(b) shows a comparison of the trend of our average bond distance of the lowest-energy structures as a function of size when compared to those obtained from the MM structures. It is evident that the empirical potential predicts slightly more expanded structures in this size range. We calculated the normal-mode frequencies with the MM structures obtaining spectra very different to ours shown in Fig. 5. For example, the normal frequencies for Ca_3 are 101 and 144 cm,[1] which are higher than our results in Table II. The discrepancy of MM frequencies with our B3PW91 results indicates that this model potential tends to stiffen the cluster structures.

V. HIGHER-ENERGY ISOMERS AND STRUCTURAL TRANSITIONS

A harmonic analysis of several thermodynamic functions was carried out based on the normal-mode frequencies. For example, the free-energy, internal energy, and vibrational specific heat were calculated for all the known isomers reported in Tables II and III of Ca_3 through Ca_{13}. Figures 9(a) and 9(b) depict the size dependence of the free energy per

atom and specific heat at 300 and 500 K (circles and crosses, respectively).

We found in this size range that the second to lowest-energy isomer of Ca_{12} (C_s) becomes more stable at a transition temperature $T_S = 317$ K. This structural transition temperature was defined as the temperature where there is a crossing of the free energy associated to two of the three Ca_{12} isomers (see Table III and Fig. 2). Figure 10(a) depicts the free energy of these three isomers as a function of temperature and the crossing point where the transition occurs. Additionally, we calculated the internal energy and the specific heat for Ca_{12}. Figures 10(b) and 10(c) show the behavior of these quantities at temperatures near T_S. In producing these two plots a broadening algorithm was used to smooth the abrupt change of the functions at the transition temperature. Below T_S the decorated twinned pentagonal bipyramid structure is preferred, and above T_S the decorated anticube structure prevails. Notice, that there is no temperature driven transition to the third-to-lowest isomer (incomplete icosahedron) within the harmonic frequency approach. This would mean that the icosahedral growth is not favored by temperature, but instead elements of cubic symmetry that span around a central atom (Ca_{10} through Ca_{12}) are more favorably enhanced at temperatures slightly above room temperature. No structural transition was detected for Ca_{13}, or for clusters smaller than Ca_{12}. Similar structural transitions might take place for cluster sizes larger that $N=13$.

VI. CONCLUSION

In this paper we have presented an analysis of small calcium clusters up to Ca_{13} using the hybrid DFT approach that includes HF calculation of the exchange energy and local and nonlocal correlation energy functionals provided by Perdew-Wang. We have determined the structure, binding energies, and harmonic frequencies of vibration for several isomers at each cluster size up to Ca_{13}. The lowest-energy

structures of Ca_6 and Ca_{10} through Ca_{13} had not been reported before as global geometries for calcium clusters. We predict that there are two paths of cluster growth. At almost zero temperature, clusters grow by twinning pentagonal bipyramids as the building block, while at temperatures closely above room temperature, clusters grow building shells of atoms around a central atom with local cubic symmetry. For Ca_{12}, instead of the icosohedron-minus-one-atom expected structure, we found that this structure is not reachable within the temperature range studied here (below 500 K). Instead the Ca_{12} lowest-energy isomer is a structure with two twinned pentagonal bipyramids that has a decorated face. We also found that this isomer undergoes a structural transition at about 317 K and becomes an isomer with local cubic symmetry elements as depicted in Fig. 2 (C_s because of slight distortions). The metallic character of calcium is far from being attained at Ca_{13} because the HOMO-LUMO energy difference is 0.8 eV, a value that is very large when compared to the small gap of 0.03 eV observed in bulk fcc calcium. The average nearest-neighbor interatomic distances for calcium clusters with $N>4$ vary between 3.82 and 3.89 Å, just slightly less than the 3.92 Å found in the fcc crystal.

Calcium is a very reactive element and combines readily with oxygen. Therefore studies of pure calcium clusters are challenging systems for experimental findings. In this direction the predictive content of this paper should be helpful. The energy barriers of various isomerization reaction paths are reported, indicating that for very small clusters, these reactions will not take place at room temperature, favoring instead oxidation mechanisms.

TABLE V. Normal-mode frequencies for the isomers of Ca_6 through Ca_9 reported in Table III.

	Sym	ν (cm^{-1})
Ca_6	C_{2v}	48.0(A_1), 68.5(A_2), 69.0(B_1), 86.4(A_1), 92.8(B_2), 97.0, 100.0(B_2), 100.9, 104.1(B_1), 119.1(B_2), 124.4(A_1), 157.6(A_1)
Ca_7	D_{5h}	74.6(E_2''), 77.8(E_1'), 95.8(A_2''), 105.1(E_2'), 107.3(E_1''), 111.0(A_1'), 116.8(E_2'), 137.6(E_1'), 167.8(A_1')
Ca_8	C_s	43.6(A''), 60.3(A'), 70.2(A'), 72.5(A''), 88.0(A'), 93.4(A'), 94.4(A''), 99.7(A''), 101.5(A'), 104.9(A'), 107.7(A'), 110.7(A''), 116.1(A''), 120.3(A'), 121.7(A'), 133.4(A''), 146.1(A'), 151.9(A')
Ca_9	C_{2v}	48.7(B_2), 53.2(A_1), 59.0(A_2), 80.8(A_1), 83.0(B_1), 84.3(A_2), 87.0(B_2), 93.4(A_1), 100.6, 100.6, 102.1(A_2), 103.9(B_1), 108.9(A_1), 113.1(A_1), 115.5(B_1), 119.4(B_2), 124.6(A_2), 128.6(A_1), 142.8(A_1), 149.8(B_2), 165.1(B_1)

TABLE VI. Normal-mode frequencies for the isomers of Ca_{10} through Ca_{13} reported in Table III.

	Sym	ν (cm^{-1})
Ca_{10}	C_{4v}	10.0(B_1), 35.7(E), 68.2(A_2), 74.5(E),75.8(B_1), 81.0(E), 89.4(E), 98.3(A_1), 101.9(B_1), 112.2(E), 122.0(A_1), 126.2(B_1), 126.3(A_1), 128.8(E), 134.6(B_2), 197.9(A_1), 215.5(E)
Ca_{11}	D_{4d}	48.7(E), 50.9, 55.8, 56.1, 62.4(E), 65.6, 71.3, 71.5, 74.8(E), 77.7, 88.9(E), 102.8, 103.0(E), 112.0, 126.0, 128.5(E), 130.8(E), 198.9, 219.4(E)
	C_1	41.0, 47.2, 52.9, 67.8, 74.4, 81.4, 83.0, 83.9, 88.3, 90.7, 91.0, 95.6, 99.6, 103.2(E), 106.6, 109.6, 111.5, 114.3, 117.9, 120.9, 131.8, 138.3, 140.2, 143.6, 147.0, 148.4
Ca_{12}	C_1	43.2, 47.0, 52.9, 59.5, 63.8, 73.8, 80.4, 81.3, 84.6, 86.9, 87.4, 90.3, 94.8, 97.3, 98.6, 100.9, 101.7, 102.6, 104.3, 105.9, 112.4, 117.6, 119.3, 127.8, 131.2, 136.9, 140.4, 147.4, 150.5, 164.8
Ca_{13}	C_1	20.5, 37.3, 51.7, 55.5, 57.0, 64.4, 75.0, 76.3, 82.2, 84.0, 86.3, 89.1, 89.9, 92.8, 93.9, 96.6, 99.0, 101.3, 103.6, 105.4, 107.9, 111.3, 111.7, 117.5, 119.8, 122.8, 128.0, 132.3, 138.9, 144.7, 159.8, 161.9, 180.3

APPENDIX: VIBRATIONAL FREQUENCIES OF Ca_6 THROUGH Ca_{13}

Determination of vibrational frequencies and its symmetry identification is a lengthy calculation. It is important to report these frequencies because they can be used in further quasiharmonic analysis of properties not studied in this paper. These frequencies might also be used to develop model potentials to represent calcium clusters. Tables V and VI contain the harmonic frequencies of vibration for all the stable isomers reported in Table III. A visual representation of the frequency spectrum as a function of cluster size is provided in Fig. 5 giving the trend for the formation of the phonon band in the bulk calcium.

[1] L. A. Heinebrodt, Ph.D. thesis, Universität Stuttgart, 1999; T. P. Martin, U. Naeher, T. Bergmann, H. Goelich, and T. Lange, Chem. Phys. Lett. **183**, 119 (1991).

[2] W. J. Balfour and R. Whitlock, Can. J. Phys. **53**, 472 (1975).

[3] C. R. Vidal, J. Chem. Phys. **72**, 1864 (1980).

[4] S. Sugano and H. Koizumi, *Microcluster Physics* (Springer-Verlag, New York, 1998).

[5] I.e., papers in *Theory of Atomic and Molecular Clusters*, edited by J. Jellinek (Springer-Verlag, New York, 1999).

[6] C. H. Chien, E. Blaisten-Barojas, and M. R. Pederson, Phys. Rev. A **58**, 2196 (1998).

[7] R. O. Jones, J. Chem. Phys. **71**, 1300 (1979).

[8] H. Stoll, J. Flad, E. Golka, and Th. Kruger, Surf. Sci. **106**, 251 (1981).

[9] G. Pacchioni and J. Koutecky, Chem. Phys. **71**, 181 (1982).

[10] G. Pacchioni and J. Koutecky, J. Chem. Phys. **77**, 5850 (1982).

[11] T. J. Lee, A. P. Rendell, and P. R. Taylor, Theor. Chim. Acta **83**, 165 (1992).

[12] C. W. Bauschlicher, Jr., P. S. Bagus, and B. N. Cox, J. Chem. Phys. **77**, 4032 (1982).

[13] P. S. Bagus, C. J. Nelin, and C. W. Bauschlicher, Jr., Surf. Sci. **156**, 615 (1985).

[14] J. N. Murrell and R. E. Mottram, Mol. Phys. **69**, 571 (1990).

[15] J. E. Hearn and R. L. Johnston, J. Chem. Phys. **107**, 4674 (1997).

[16] W. Kohn and L. J. Sham, Phys. Rev. A **140**, 1133 (1965).

[17] A. D. Becke, J. Chem. Phys. **98**, 5648 (1993).

[18] J. P. Perdew, J. A. Chevary, S. H. Vosko, K. A. Jackson, M. R. Pederson, D. J. Singh, C. Fiolhais, Phys. Rev. B **46**, 6671 (1992).

[19] J. P. Perdew, K. Burke, and Y. Wang, Phys. Rev. B **54**, 16 533 (1996).

[20] J. P. Blaudeau, M. P. McGrath, L. A. Curtiss, and L. Radom, J. Chem. Phys. **107**, 5016 (1997).

[21] F. van Duijneveldt, J. van Duijneveldt-van de Rijdt, and J. van Lenthe, Chem. Rev. **94**, 1873 (1994).

[22] R. Krishnan and J. A. Pople, Int. J. Quantum Chem. **14**, 91 (1978).

[23] M. J. Frisch *et al.*, Gaussian Inc., Pittsburgh, PA, 1998.

[24] M. R. Pederson and K. A. Jackson, Phys. Rev. B **41**, 7453

(1990).

[25] D. V. Porezag, Ph.D. thesis, Technische Universität Chemnitz-Zurickau, 1997. Basis sets are available at http://archv.tu-chemnitz.de/pub/1997/0025

[26] K. P. Huber and G. Herzberg, *Constants of Diatomic Molecules* (Van Nostrand Reinhold, New York, 1979).

[27] J. W. McCaffrey, J. R. Anderson, and D. Papaconstantopoulos, Phys. Rev. B **7**, 674 (1973).